AIP | Journal of Mathematical Physics

Power statistics for wave propagation in onedimension and comparison with radiative transport theory. II

W. Kohler and G. C. Papanicolaou

Citation: Journal of Mathematical Physics **15**, 2186 (1974); doi: 10.1063/1.1666600
View online: http://dx.doi.org/10.1063/1.1666600
View Table of Contents: http://scitation.aip.org/content/aip/journal/jmp/15/12?ver=pdfcov
Published by the AIP Publishing

Power statistics for wave propagation in one-dimension and comparison with radiative transport theory. II

W. Kohler

Department of Mathematics, Virginia Polytechnic Institute and State University, Blacksburg, Virginia 24061

G. C. Papanicolaou*

Courant Institute of Mathematical Sciences, New York University, New York, New York 10012
(Received 10 April 1974)

We consider the one-dimensional problem of a slab having a random index of refraction and illuminated from within by a point source. We compute the expected value and the fluctuations of both the total power and power flux. These quantities, which are functions of the slab width, source location, and observation point, are determined in the limit of weak refractive index fluctuations and large slab thickness. We compare the expected values of total intensity and flux with the predictions of radiative transport theory. We also compare the results of both theories with numerical simulations.

1. INTRODUCTION AND SUMMARY

This work is a continuation and extension of previous work by us,[1] which we shall refer to as I in the text. Except in the derivations of Sec. 4, where we rely on some of the analysis developed in I, the description of the problem and the results are self-contained here.

We consider a one-dimensional medium with a random index of refraction that fluctuates slightly from an expected value of unity. This medium occupies the interval $[0, l]$. The regions to the right of l and to the left of 0 are assumed to have a constant index of refraction equal to one. A time-harmonic point source is located within the interval $[0, l]$. We are interested in the statistical properties of the resulting wave field throughout the medium. More specifically, we are interested in the mean value or expectation of the total power (intensity) of the waves, the expectation of the power flux and the fluctuations of the intensity and flux about their mean values.

The formulation of the above as a transmission line problem was carried out in I, and it leads to the same mathematical considerations. This is also true for the propagation of the fundamental mode in a waveguide with random inhomogeneities. All computations presented in this work will deal with what was termed the matched case in I, i.e., the medium in the absence of random perturbations, has an index of refraction equal to unity everywhere on $(-\infty, \infty)$. The extension of the new results to the mismatched case, however, can be carried out without difficulty as we indicate in Sec. 4.

We study the above problem in the asumptotic limit of weak fluctuations of the refractive index and large slab thicknesses. The fluctuations are characterized by a small parameter ϵ while the thickness $l \sim 1/\epsilon^2$. The wavelength in the unperturbed medium and the correlation length of the random inhomogeneities are assumed to be of order one relative to ϵ. We shall refer to the asymptotic limit as the diffusion limit. A formal description of this limit is given in Ref. 2. More mathematical descriptions are presented in Refs. 3, 4, while additional references are cited in Refs. 3, 4 and I. References 5 and 6 can be consulted for related information.

Our results are the following. First, we compute in the diffusion limit the expectation of the total power or intensity of the wave field as a function of the scaled width of the slab of the random medium, the scaled source location and the scaled observation point. From this expression, in turn, we determine the expectation of the power flux. Thus, we generalize the results of I, wherein the source was located at the left end of the slab, i.e., radiation was incident from the left. This latter problem has also been treated by Gazaryan[7] and Lang.[8] Rubin[9,10] has considered the analogous problem of wave propagation through a one-dimensional randomly disordered crystal while Halperin[11] has also dealt with a similar problem in his calculation of the spectral density for a particle in a one-dimensional random potential.

Our second result is the computation in the diffusion limit of the fluctuations of the total power about its mean value as a function of the scaled slab width, scaled source location, and scaled observation point. We again use this expression to determine, as a special case, the fluctuations of the power flux. These quantities, which were not computed in I, provide important insights into the basic nature of wave propagation in random media. Marcuse[12] has also computed power fluctuations but within the forward scattering approximation, and so his results differ from ours.

We compare our results for the expected total power with the predictions of radiative transport theory. This is a phenomenological theory, due to Schuster,[13] that leads to simple equations for the total intensity and flux of radiation through an inhomogeneous medium. As in I, we find discrepancies between the stochastic and transport theories and conclude that radiative transport theory in one-dimension cannot be derived from a stochastic wave theory in the diffusion limit as one might expect from physical considerations (cf. references in I). Furthermore, intensity fluctuations in the interior can be so large as to render the mean intensity in the interior a relatively unimportant quantity.

We also compare our results with the results of numerical simulations. The predictions of the stochastic theory for the mean value and fluctuations of both the total power and power flux are found to be in good agreement with the simulation data.

Section 2 presents the formulation of the problem and a delineation of our results. Section 3 compares these

diffusion limit results both with those of radiative transport theory and the results of numerical simulations. Graphs are presented which illustrate the behavior of the quantities of interest; these graphs are discussed in Sec. 3. We also briefly indicate how our results can be applied to the case where the physical configuration remains fixed while frequency or wavenumber is permitted to vary. Section 4 presents a derivation of the results. This derivation relies both upon theorems established in Refs. 3, 4 and also upon the formulation in I. Therefore, some details are omitted.

We take this opportunity to refer to the work of Besieris and Tappert[14] in connection with the pulse problem discussed in Sec. 9 of I. Our formula for the pulse-spreading factor [below (I. 9.47)] agrees, up to a factor 3/2, with their results. In our formula, as well as in (I. 9.44), the factor $\int_0^\infty R(s)\cos 2ks\,ds$ is set equal to one so that (I. 9.44) is in fact dimensionally correct. Besieris and Tappert treat the problem in the forward scattering approximation but, as (I. 9.8) and (I. 9.9) indicate, backscattering is negligible in the diffusion limit as well.

2. FORMULATION OF THE PROBLEM AND STATEMENT OF RESULTS

Let $u(x)$ denote the complex-valued scalar wave field at location $x\in(-\infty,\infty)$ with the time dependence $\exp(-i\omega t)$ omitted throughout. We assume that $u(x)$ satisfies the following equation and boundary conditions:

$$\frac{d^2u(x)}{dx^2}+k^2[1+\epsilon\mu(x)]u(x)=i2k\,\delta(x-y),\quad 0\le x,y\le l, \tag{2.1}$$

$$u(x)=T_+\exp(ikx),\quad x\ge l,\quad u(x)=T_-\exp(-ikx),\quad x\le 0, \tag{2.2}$$

$$u(x)\text{ and }\frac{du(x)}{dx}\text{ continuous}, \tag{2.3}$$

$$E\{\mu(x)\}=0,\quad R(z)=E\{\mu(x+z)\mu(x)\}. \tag{2.4}$$

Here k is the free space wavenumber, $\mu(x)$ is a wide-sense stationary random process satisfying (2.4)[15] (where $E\{\cdot\}$ denotes expected value) and ϵ is a small parameter characterizing the fluctuations of the refractive index. $T_+(y,l)$ and $T_-(y,l)$ are the complex-valued right and left transmission coefficients. These coefficients depend upon y, the source location, and l, the width of the random medium, as does the wave field $u=u(x,y,l)$. In general, we will not display this dependence upon y and l explicitly.

As in (I. 2.15)[16] we define the complex valued functions $A(x,y,l)$ and $B(x,y,l)$ by

$$u(x)=\exp(ikx)A(x)+\exp(-ikx)B(x),$$

$$\frac{du(x)}{dx}=ik[\exp(ikx)A(x)-\exp(-ikx)B(x)] \tag{2.5}$$

so that

$$A(x)=\tfrac{1}{2}\exp(-ikx)\left(u(x)+\frac{1}{ik}\frac{du(x)}{dx}\right),$$

$$B(x)=\tfrac{1}{2}\exp(ikx)\left(u(x)-\frac{1}{ik}\frac{du(x)}{dx}\right). \tag{2.6}$$

We interpret $A(x)$ and $B(x)$ as the "slowly varing" complex amplitudes of right and left propagating waves whose sum composes the wave field $u(x)$. From (2.1)–(2.3) and (2.5) we see that $A(x)$ and $B(x)$ satisfy the following stochastic boundary value problem:

$$\frac{dA(x)}{dx}=\frac{\epsilon ik\mu(x)}{2}[A(x)+B(x)\exp(-i2kx)],$$

$$\frac{dB(x)}{dx}=\frac{-\epsilon ik\mu(x)}{2}[\exp(i2kx)A(x)+B(x)],\quad 0\le x\le l,\ x\ne y, \tag{2.7}$$

$$A(y+0,y,l)-A(y-0,y,l)=\exp(-iky),$$

$$B(y+0,y,l)-B(y-0,y,l)=-\exp(iky),\quad 0\le y\le l, \tag{2.8}$$

$$A(0,y,l)=B(l,y,l)=0. \tag{2.9}$$

The arguments $y+0$ and $y-0$ in jump conditions (2.8) refer to the limits as x tends to y from the right and left respectively. Note that $A(x,y,l)$, $B(x,y,l)$, and $u(x,y,l)$ are random functions which depend upon ϵ. We shall sometimes use a superscript, i.e., $A^{(\epsilon)}$, $B^{(\epsilon)}$, $u^{(\epsilon)}$, to denote this dependence.

From (2.6) and (2.7)–(2.9) it follows that

$$|T_+^{(\epsilon)}(y,l)|^2=|A^{(\epsilon)}(x,y,l)|^2-|B^{(\epsilon)}(x,y,l)|^2$$

$$=\frac{1}{i2k}\left(\bar u^{(\epsilon)}\frac{du^{(\epsilon)}}{dx}-u^{(\epsilon)}\frac{d\bar u^{(\epsilon)}}{dx}\right),\quad x>y, \tag{2.10}$$

$$|T_-^{(\epsilon)}(y,l)|^2=-|A^{(\epsilon)}(x,y,l)|^2+|B^{(\epsilon)}(x,y,l)|^2$$

$$=-\frac{1}{2ik}\left(\bar u^{(\epsilon)}\frac{du^{(\epsilon)}}{dx}-u^{(\epsilon)}\frac{d\bar u^{(\epsilon)}}{dx}\right),\quad x<y. \tag{2.11}$$

The functions $|T_+|^2$ and $|T_-|^2$ represent the power flux to the right and to the left of the source, respectively. Since the medium is lossless, the two fluxes are independent of the location of the observation point and depend only upon the location of the source point and the width of the random medium. We define the total power or intensity by

$$J^{(\epsilon)}(x,y,l)=|A^{(\epsilon)}(x,y,l)|^2+|B^{(\epsilon)}(x,y,l)|^2$$

$$=\tfrac{1}{2}\left(|u^{(\epsilon)}|^2+\frac{1}{k^2}\left|\frac{du^{(\epsilon)}}{dx}\right|^2\right). \tag{2.12}$$

This quantity depends on the observation point, source point, and the width of the random medium. Note that when $\epsilon=0$, i.e., there are no random inhomogeneities, then $u(x)=\exp(ik|x-y|)$, $|A|^2-|B|^2=\mathrm{sgn}(x-y)$, and $|A|^2+|B|^2=1$. It follows from (2.9) that

$$|T_+^{(\epsilon)}(y,l)|^2=J^{(\epsilon)}(l,y,l), \tag{2.13}$$

$$|T_-^{(\epsilon)}(y,l)|^2=J^{(\epsilon)}(0,y,l),\quad 0\le y\le l. \tag{2.14}$$

Therefore, it is not necessary to compute the power fluxes separately since they can be obtained from $J^{(\epsilon)}$.

By letting $y\to 0$, $y\le x\le l$ in (2.7)–(2.9) we recover problem (I. 2.6), (I. 2.7) with $\Gamma_g=\Gamma_l=0$. Therefore, $J^{(\epsilon)}(x,0,l)$ is the function that was considered in I, i.e., total power or intensity as a function of the observation point and width of the random medium, with plane wave illumination of the medium from the left. Note that $J^{(\epsilon)}(l,0,l)$ is the power transmission coefficient for this configuration. All relevant information about power transport is contained, therefore, in the random function $J^{(\epsilon)}(x,y,l)$, $0\le x,y\le l$.

We shall now state our results. Let τ, ξ, and η be defined as follows:

$$\tau=\epsilon^2 l, \quad \xi=\epsilon^2 y-\tau/2, \quad \eta=\epsilon^2 x-\tau/2. \tag{2.15}$$

These variables are the scaled width of the random medium, the scaled distance of the source from the midpoint, and the scaled distance of the observation point from the midpoint, respectively. The limit $\epsilon \downarrow 0$ with τ, ξ, and η fixed is called the diffusion limit. The mean power or intensity in the diffusion limit is defined by

$$MJ(\tau,\xi,\eta)=\lim_{\epsilon\downarrow 0} E\{J^{(\epsilon)}([\tau/2+\eta]/\epsilon^2,[\tau/2+\xi]/\epsilon^2,\tau/\epsilon^2)\}. \tag{2.16}$$

As our first result, we assert that this limit exists and that MJ is given by the following formula:

$$MJ(\tau,\xi,\eta)=\exp(3\alpha\tau/4-\alpha|\xi-\eta|)\int_{-\infty}^{\infty}\frac{\exp(-t^2\alpha\tau)\pi\sinh\pi t}{t\cosh^2\pi t}$$
$$\times[(t^2+\tfrac{1}{4})\cos 2t\alpha(\xi+\eta)+(t^2-\tfrac{1}{4})\cos 2t\alpha(\tau-|\xi-\eta|)$$
$$+t\sin 2t\alpha(\tau-|\xi-\eta|)]\,dt, \tag{2.17}$$

where $\tau\geq 0$, $-\tau/2\leq\xi,\eta\leq\tau/2$, and

$$\alpha=\tfrac{1}{2}k^2\int_0^\infty R(s)\cos 2ks\,ds. \tag{2.18}$$

From (2.17) and (2.18) it follows that MJ depends on k and the correlation function $R(s)$ [cf. (2.4)] through the parameter α which is the value of the power spectrum of $k\mu$ at wavenumber $2k$. For brevity, we refer to MJ as a function of τ, ξ, and η although it actually is a function of $\alpha\tau$, $\alpha\xi$, and $\alpha\eta$. Observe that MJ is a symmetric function of ξ and η (i.e., it obeys the principle of reciprocity) and is invariant under the transformation $\xi\to-\xi$, $\eta\to-\eta$.

When $\xi=-\tau/2$, i.e., the source is at the left end of the random medium, we recover formula (I. 6.32)[17] with $\theta_g=\theta_l=0$.

$$MJ(\tau,-\tau/2,\eta)=\exp(\alpha\tau/4-\alpha\eta)\int_{-\infty}^{\infty}\frac{\exp(-t^2\alpha\tau)\pi t\sinh\pi t}{\cosh^2\pi t}$$
$$\times\left(\cos t\alpha(\tau-2\eta)+\frac{\sin t\alpha(\tau-2\eta)}{2t}\right)dt,$$
$$-\tau/2\leq\eta\leq\tau/2. \tag{2.19}$$

Because of the symmetry $MJ(\tau,-\tau/2,\eta)=MJ(\tau,\eta,-\tau/2)$ it follows that $MJ(\tau,\xi,-\tau/2)$ is given by (2.19) with ξ replacing η. However, from (2.14) we conclude that

$$MJ(\tau,\xi,-\tau/2)=\lim_{\epsilon\downarrow 0} E\{|T_-^{(\epsilon)}([\tau/2+\xi]/\epsilon^2,\tau/\epsilon^2)|^2\}. \tag{2.20}$$

Thus, the mean power flux to the left as a function of source location and slab width coincides in the diffusion limit with the mean total power in the interior at the former source location when the slab is now excited by a source at the left end. Analogous consequences of reciprocity exist for T_+, but no additional computations are needed in view of obvious symmetry about the midpoint of the slab. When $\xi=-\tau/2$ and $\eta=\tau/2$, we obtain the mean power transmission coefficient (cf. references in I, Sec. 7).

$$MJ(\tau,-\tau/2,\tau/2)=\exp(-\alpha\tau/4)\int_{-\infty}^{\infty}\exp(-t^2\alpha\tau)\frac{\pi t\sinh\pi t}{\cosh^2\pi t}\,dt. \tag{2.21}$$

Our second result concerns the fluctuations of the total intensity $J^{(\epsilon)}$ in the diffusion limit. We define $KJ(\tau,\xi,\eta)$ as follows:

$$KJ(\tau,\xi,\eta)=\lim_{\epsilon\downarrow 0} E\{(J^{(\epsilon)}([\tau/2+\eta]/\epsilon^2,[\tau/2+\xi]/\epsilon^2,\tau/\epsilon^2))^2\}. \tag{2.22}$$

The fluctuation in the total power is then given by

$$FJ(\tau,\xi,\eta)=[KJ(\tau,\xi,\eta)-(MJ(\tau,\xi,\eta))^2]^{1/2}, \tag{2.23}$$
$$\tau\geq 0,\ -\tau/2\leq\xi,\ \eta\leq\tau/2.$$

We find that

$$KJ(\tau,\xi,\eta)=\frac{\exp(15\alpha\tau/4-4\alpha|\eta-\xi|)}{8}\int_{-\infty}^{\infty}\frac{\pi t\sinh\pi t}{\cosh^2\pi t}\exp(-t^2\alpha\tau)$$
$$\times\frac{(t^2+\frac{1}{4})}{(t^2+1)^2}\left((t^2+\tfrac{3}{4})\exp(-2\alpha(\tau-2\sigma\eta))+(t^2+\tfrac{5}{4})\right.$$
$$\left.\times\cos 2t\alpha(\tau-2\sigma\eta)+(t^2+\tfrac{3}{4})\frac{\sin 2t\alpha(\tau-2\sigma\eta)}{t}\right)$$
$$\times\left[(t^2+\tfrac{1}{4})\exp(-2\alpha(\tau+2\sigma\xi))+3\left((t^2+\tfrac{5}{4})\right.\right.$$
$$\left.\left.\times\cos 2t\alpha(\tau+2\sigma\xi)+(t^2+\tfrac{3}{4})\frac{\sin 2t\alpha(\tau+2\sigma\xi)}{t}\right)\right]dt,$$
$$\sigma\equiv\operatorname{sgn}(\eta-\xi). \tag{2.24}$$

Observe that $KJ(\tau,\xi,\eta)$ is invariant under the transformation $\xi\to-\xi$, $\eta\to-\eta$. However, as Eq. (2.24) indicates, the second moment of the total intensity is not invariant under an interchange of ξ and η, the source and observation points.

When $\xi=-\tau/2$, (2.24) reduces to

$$KJ(\tau,-\tau/2,\eta)=\frac{\exp(7\alpha\tau/4-4\alpha\eta)}{2}\int_{-\infty}^{\infty}\frac{\pi t\sinh\pi t}{\cosh^2\pi t}$$
$$\times\exp(-t^2\alpha\tau)\frac{(t^2+\frac{1}{4})}{(t^2+1)}\ (t^2+\tfrac{3}{4})\exp(-2\alpha(\tau-2\eta))+(t^2+\tfrac{5}{4})$$
$$\times\cos 2t\alpha(\tau-2\eta)+(t^2+\tfrac{3}{4})\frac{\sin 2t\alpha(\tau-2\eta)}{t}\ dt. \tag{2.25}$$

From (2.25), (2.19), and (2.23), we obtain the power fluctuations at observation point η, $-\tau/2\leq\eta\leq\tau/2$, when the source is at the left end; this solves the power fluctuation problem associated with I. Finally, when $\xi=-\tau/2$ and $\eta=\tau/2$, we obtain

$$KJ(\tau,-\tau/2,\tau/2)=\exp(-\alpha\tau/4)\int_{-\infty}^{\infty}\frac{\pi t\sinh\pi t}{\cosh^2\pi t}$$
$$\times\exp(-t^2\alpha\tau)\,(t^2+\tfrac{1}{4})\,dt. \tag{2.26}$$

Therefore, from (2.26), (2.21), and (2.23) we obtain the fluctuation in the mean power transmission coefficient.

In Figs. 1a—12a we plot the mean total power or intensity MJ and in Figs. 1b—12b the intensity fluctuations FJ as functions of the observation point $\alpha\eta$ for a selection of slab widths and source locations. In Figs. 13a and 13b we plot the mean power transmission coefficient and its fluctuations as a function of slab thickness with the source at the left end. Observe that we have only considered source locations over half the slab width (i.e., $\xi=-\tau/2, -\tau/4, 0$). Since MJ, KJ, and therefore

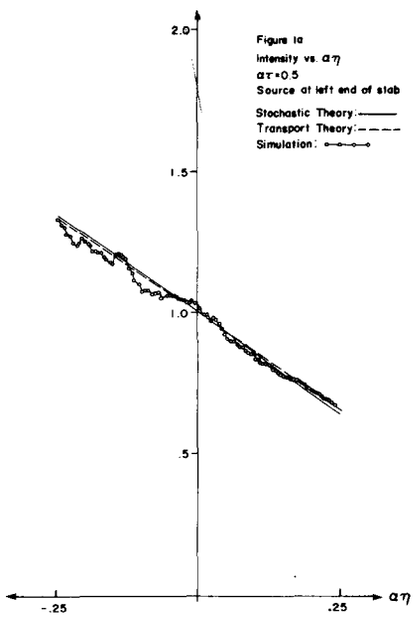

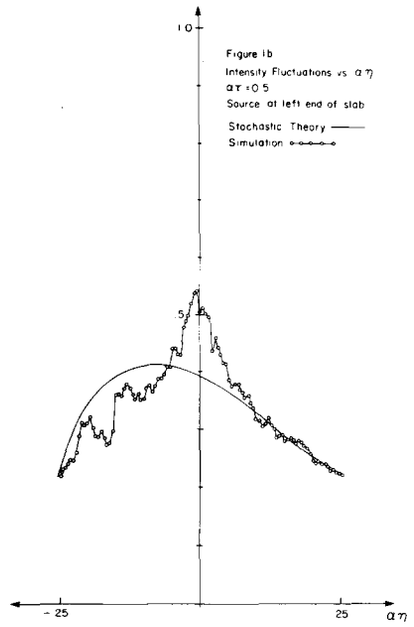

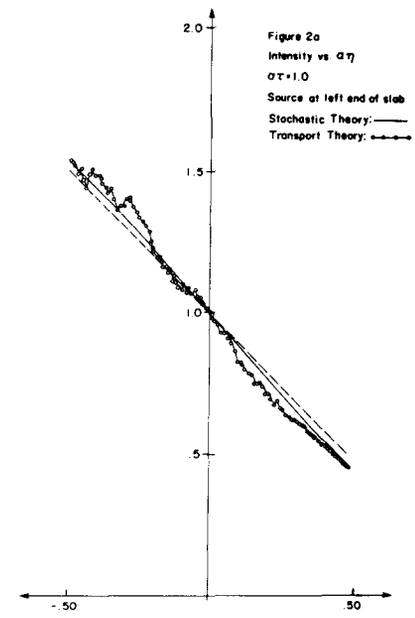

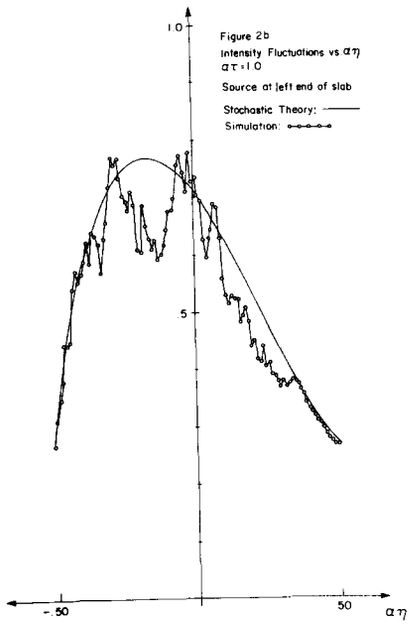

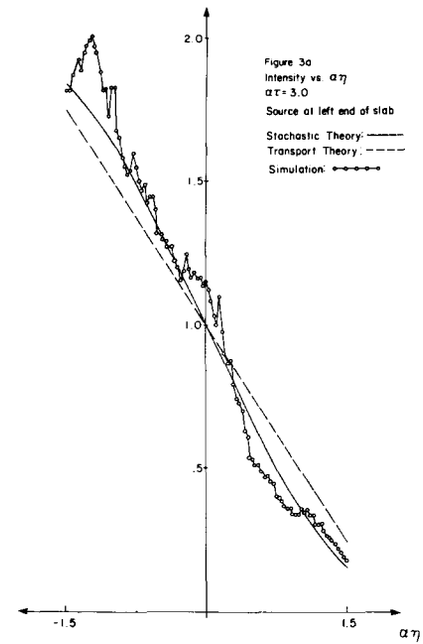

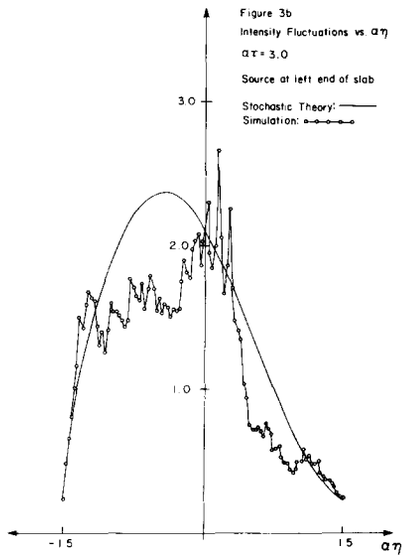

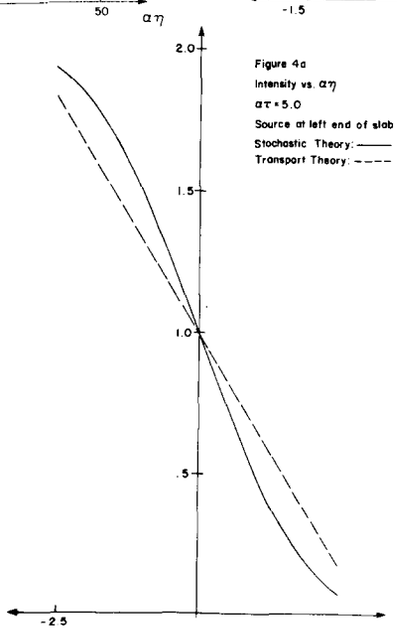

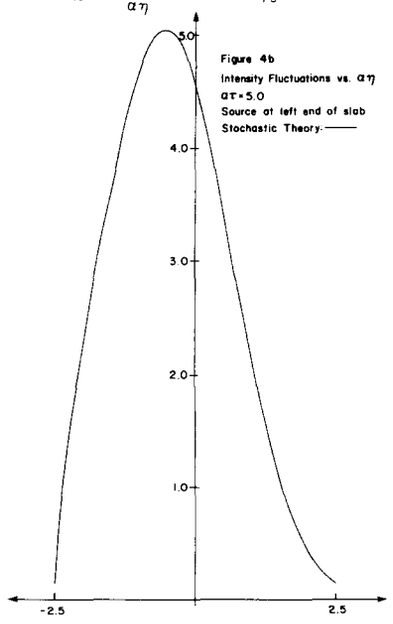

FIGS. 1–4.

FJ are invariant under the transformation $\eta \to -\xi$, $\eta \to -\eta$, the plots for the corresponding source locations in the other half of the slab (i.e., $\xi = \tau/4, \tau/2$) can be obtained by reflecting the presented curves about the vertical axis.

On these graphs, we have superimposed the results of random simulations conducted to verify the theory; the agreement is good. Observe that for the three source locations considered, the maximum value of the mean intensity occurs at the source point. As one moves away from the source point, the mean intensity decreases monotonically. For a fixed slab thickness, the value of the mean intensity at the source point increases as the source point is moved from the slab end toward the center. If, on the other hand, we increase the slab thickness while keeping the relative source position fixed (i.e., $\xi/\tau = \text{const.}$) the mean intensity at the source point is again seen to increase.

When the slab is excited at the left end, the intensity fluctuations at the left and right ends of the slab are equal (cf. Figs. 1b—4b). This is to be expected since the intensities at the left and right ends of the slab correspond to one plus the power reflection coefficient and the power transmission coefficient, respectively. Since the random medium is nondissipative, the two intensities must sum to two; thus the variance of the two slab end intensities must be equal. Observe that the peak fluctuations (with source at left end) occur in the slab interior between the left end and center. As the slab width $\alpha\tau$ is increased, the peak fluctuation also increases.

When the source is positioned in the slab interior, the peak fluctuations occur at the source point and for a given slab thickness, they are considerably greater than those occuring when the slab is excited at the end. Moreover, as the slab thickness is increased with the relative source position held fixed (i.e., $\xi/\tau = \text{const.}$), the fluctuations build up very rapidly.

On the basis of the results described above and displayed in the figures we may conclude the following:

For $\alpha\tau$ small, say less than one, the intensity fluctuations are relatively small and the mean intensity behaves in much the same way as the predictions of radiative transport theory (cf. Sec. 3). For $\alpha\tau > 2$, however, the intensity fluctuations in the interior can be very large, especially when the source is also located in the interior. In this case, neither the mean intensity of the stochastic theory nor that of the phenomenological transport theory give any insight into the extremely fluctuating character of the fields. On the other hand, away from the source point and near the slab extremities, the intensity fluctuations remain moderate even when $\alpha\tau$ is large. This is particularly true when the slab is illuminated at one end. Therefore, the mean of the power reflection and transmission coefficients (cf. Fig. 13) are stable quantities and the comparison with transport theory is meaningful. The enormous size of the fluctuations in the interior was unexpected and indeed surprising.

In Sec. 3, we shall discuss these results in more detail and compare them with transport theory.

3. COMPARISON WITH RADIATIVE TRANSPORT THEORY AND DESCRIPTION OF THE RESULTS

Radiative transport theory is a phenomenological theory that views the propagation and scattering of radiation as an incoherent process. This theory was first applied to the one-dimensional problem by Schuster.[13] We shall now outline the transport theory analog of problem (2.1)—(2.4) and compare the corresponding solution with the results of Sec. 2, as we did in Sec. 8 of I.

Let us assume that a scattering medium, occupying the interval $[-\tau/2, \tau/2]$, is excited from within by a point source whose distance from the center of the slab is denoted by ξ. Let η represent the distance of the observation point from the center of the slab. We shall assume a steady state condition and a conservative medium. Let $I^+(\tau, \xi, \eta)$ and $I^-(\tau, \xi, \eta)$ represent the intensities of radiation at location η, propagating in the positive and negative η directions, respectively. Assume that over an interval of length $d\eta$, there occurs a backscattering of radiation equal to $\alpha I^+ d\eta$ and a forward scattering equal to $\alpha I^- d\eta$. Then, a conservation of energy argument leads to the following equations:

$$\frac{d}{d\eta} I^+ = \frac{d}{d\eta} I^- = -\alpha (I^+ - I^-), \tag{3.1}$$

$$I^+(\tau, \xi, -\tau/2) = I^-(\tau, \xi, \tau/2) = 0, \tag{3.2}$$

$$I^\pm(\tau, \xi, \xi + 0) - I^\pm(\tau, \xi, \xi - 0) = \pm 1. \tag{3.3}$$

Boundary conditions (3.2) are a simple consequence of the fact that scattering only occurs in the interval $[-\tau/2, \tau/2]$. The notation $\xi + 0$ and $\xi - 0$ used in jump condition (3.3) again refers to limits as η approaches ξ from the right and left, respectively. The point source at location ξ is assumed to emit radiation of unit intensity. Note that the transport coefficient in (3.1) is the parameter α defined by (2.18). This choice has been justified, on the one hand, in an *a priori* manner by the heuristic arguments of Marcuse.[18] On the other hand, this choice will also be dictated in an *a posteriori* manner by the comparison of stochastic and transport theoretic predictions for small values of $\alpha\tau$.

We shall use the subscript s (for Schuster) to denote the transport theoretic quantities of interest. It follows readily from (3.1)—(3.3) that:

$$MJ_s(\tau, \xi, \eta) \equiv I^+ + I^- = [1 + \alpha(\tau + 2\sigma\xi)][1 + \alpha(\tau - 2\sigma\eta)]/(1 + \alpha\tau),$$
$$\sigma \equiv \operatorname{sgn}(\eta - \xi). \tag{3.4}$$

Noting (2.10)—(2.14), we also obtain

$$|T_{+_s}(\xi, \tau)|^2 \equiv I^+ - I^- = \frac{1 + \alpha(\tau + 2\xi)}{1 + \alpha\tau} = MJ_s(\tau, \xi, \tau/2), \quad \eta \geq \xi, \tag{3.5}$$

$$|T_{-_s}(\xi, \tau)|^2 \equiv I^- - I^+ = \frac{1 + \alpha(\tau - 2\xi)}{1 + \alpha\tau} = MJ_s(\tau, \xi, -\tau/2), \quad \eta \leq \xi. \tag{3.6}$$

We again can obtain the right and left-directed power flux by an evaluation of the total intensity at the right and left slab ends, respectively.

Let us now compare the mean total intensities MJ and MJ_s when the slab thickness is small. Assume that

$\alpha\tau \ll 1$ with $-\tau/2 \leq \xi,\ \eta \leq \tau/2$. Define

$$\beta_n \equiv \int_{-\infty}^{\infty} \frac{\pi t^{2n+1} \sinh \pi t}{\cosh^2 \pi t}\, dt, \quad n = 0, 1, 2, \cdots. \tag{3.7}$$

Using the fact that $\beta_0 = 1$, $\beta_1 = 3/4$, and $\beta_2 = 25/16$, we find the expansions of MJ and MJ_s agree to terms of order $(\alpha\tau)^3$. Specifically

$$\begin{aligned} MJ(\tau, \xi, \eta) &= 1 + \alpha\tau - 2\alpha\,|\eta - \xi| - 4\alpha^2 \xi\eta + O[(\alpha\tau)^3] \\ &= MJ_s(\tau, \xi, \eta) + O[(\alpha\tau)^3]. \end{aligned} \tag{3.8}$$

In Figs. 1—13, we present a graphical comparison of the predictions of the stochastic and radiative transport theories. The stochastic theoretic curves are drawn as solid lines while the transport theory curves are drawn as dashed lines. Also displayed on these graphs are the results of numerical simulations conducted to verify these theoretical results. Figures 1a—12a compare the intensities, i.e., MJ and MJ_s, as a function of the observation point for a variety of slab thicknesses and source locations. Figures 1b—12b present the intensity fluctuations FJ as a function of the observation point for the same selection of slab thicknesses and source locations. Note that we have not exhibited a transport-theoretic analog of FJ. Figure 13a compares the stochastic and transport theoretic transmission coefficients, i.e., $MJ(\tau, -\tau/2, \tau/2)$ and $MJ_s(\tau, -\tau/2, \tau/2)$, as functions of slab thickness while Fig. 13b presents the transmission coefficient fluctuations $FJ(\tau, -\tau/2, \tau/2)$.

Figures 1—4 correspond to a source location at the left end of the slab. For this configuration, both the stochastic and transport theoretic intensities attain their maximum values at the source point and are monotonically decreasing functions of the observation point. Both intensities are equal to unity at the slab center. For small values of $\alpha\tau$, the two intensity curves practically coincide; this is to be expected in view of (3.8). As $\alpha\tau$ increases, however, the effects of multiple scattering become more pronounced. Both intensity curves tend asymtotically toward the values 2 and 0 at the left and right slab ends, respectively. However, as $\alpha\tau$ increases, the transport theoretic intensity remains a linear function of the observation point while the stochastic intensity exhibits an increasingly nonlinear behavior. Note that, in all cases, for both theories, the intensities at the two slab ends sum to two. This is to be expected since the intensity at the left end equals one plus the power reflection coefficient while the intensity at the right end equals the power transmission coefficient. Since the random medium is conservative, the reflection and transmission coefficients must sum to unity.

In Figures 1b—4b, we present the intensity fluctuations FJ as a function of the observation point $\alpha\eta$ for the source point at the left end of the slab. As we noted in Sec. 2, the fluctuations at the two slab ends are equal. This is due to the fact that they represent the standard deviations of two random variables whose sum is a constant, i.e., 2. Observe that the largest intensity fluctuations occur in the left half of the slab; these fluctuations increase as the slab thickness increases. The occurrence of large fluctuations in the half of the slab nearest the incident excitation is, as the graphs indicate, supported by our numerical simulations. This phenomenon is also in qualitative agreement with observations made by Frisch, Froeschle, Scheidecker, and Sulem[19] based on numerical simulations that they conducted.

Figures 5—8 correspond to a source location midway between the left end and the center of the slab, i.e., $\xi = \tau/4$. Observe that the sum of the intensities at the two slab ends, i.e., $MJ(\tau, \xi, -\tau/2) + MJ(\tau, \xi, \tau/2)$ and $MJ_s(\tau, \xi, -\tau/2) + MJ_s(\tau, \xi, \tau/2)$, again equlas 2. This phenomenon occurs for an arbitrary interior source location. We shall now show that in the stochastic case there follows, as a simple consequence of jump condition (2.8), the fact that the right and left power fluxes are independent of the observation point [cf. (2.10)—(2.14)], and the diffusion limit. From (2.10), (2.11) it follows that

$$\begin{aligned} |T_+^{(\epsilon)}|^2 + |T_-^{(\epsilon)}|^2 &= |A^{(\epsilon)}(y + 0, y, l)|^2 - |A^{(\epsilon)}(y - 0, y, l)|^2 \\ &\quad + |B^{(\epsilon)}(y - 0, y, l)|^2 - |B^{(\epsilon)}(y + 0, y, l)|^2. \end{aligned} \tag{3.9}$$

Using (2.8) and (2.13)—(2.15), we obtain

$$\begin{aligned} &J^{(\epsilon)}(\tau/\epsilon^2, [\tau/2 + \xi]/\epsilon^2, \tau/\epsilon^2) + J^{(\epsilon)}(0, [\tau/2 + \xi]/\epsilon^2, \tau/\epsilon^2) \\ &\quad = 2 + 2\,\mathrm{Re}\{[\overline{A^{(\epsilon)}}(\tau/2 + \xi - 0]/\epsilon^2, [\tau/2 + \xi]/\epsilon^2, \tau/\epsilon^2) \\ &\qquad + B^{(\epsilon)}([\tau/2 + \xi + 0]/\epsilon^2, [\tau/2 + \xi]/\epsilon^2, \tau/\epsilon^2)] \\ &\qquad \times \exp[ik(\tau/2 + \xi)/\epsilon^2]\}. \end{aligned} \tag{3.10}$$

When the diffusion limit (2.16) is applied, the rapid phase variations annihilate the expected value of the second term on the right side of (3.10) and we obtain the aforementioned result. The argument for the transport theoretic case follows immediately from jump condition (3.3) and Eqs. (3.5)—(3.6).

For the source located midway between the left end and center of the slab, the peak intensity occurs at the source point. Observe that, as the slab thickness increases, the effects of multiple scattering again become increasingly important and the peak intensity predicted by the stochastic theory grows much faster than that predicted by transport theory (cf. Figs. 5a—8a). Figures 5b—8b display the intensity fluctuations corresponding to this source configuration. Observe that the intensity fluctuations at the slab ends are not equal in this case. Note also the discontinuity in the fluctuations at the source point that is very apparent for the smaller slab thicknesses (Figs. 5b, 6b) but which effectively disappears for the thicker slabs (Figs. 7b, 8b), i.e., when the source is located in the deep interior.

Figures 8—12 display the intensity and fluctuation variations corresponding to a source located at the center of the slab. The graphs display the obviously required symmetry with respect to the slab center. The peak intensity and peak fluctuations both occur at the source point. For a given slab thickness, this source location produces the largest peak values. Note, moreover, that these peak values become very large for moderate valyes of $\alpha\tau$; a peak intensity of 30 and a peak fluctuation of 5000 occur for $\alpha\tau$ equal to 5.

Figures 13a and 13b show the variation of the power transmission coefficient and power transmission coefficient fluctuations, respectively, as a function of $\alpha\tau$ for a source located at the left end of the slab. For the stochastic theory, the transmission coefficient is given by

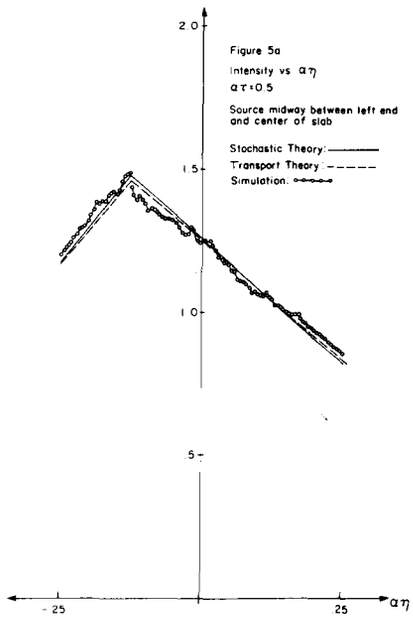

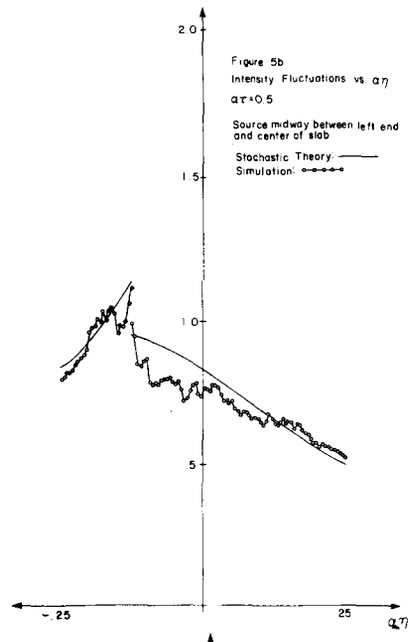

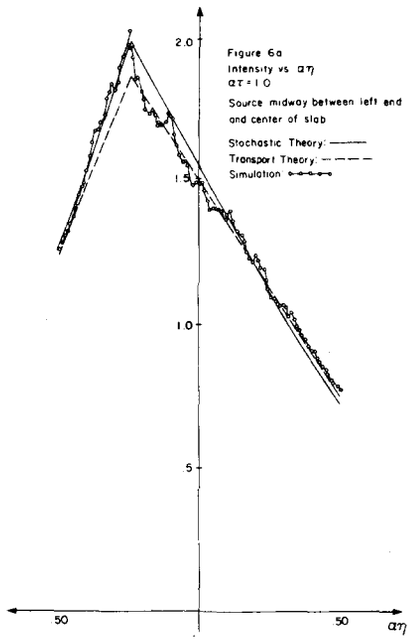

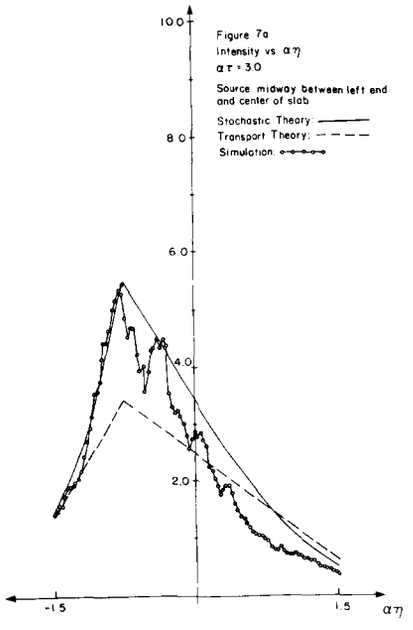

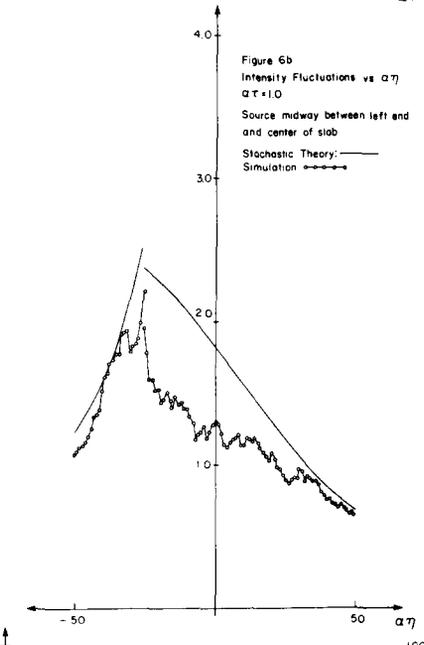

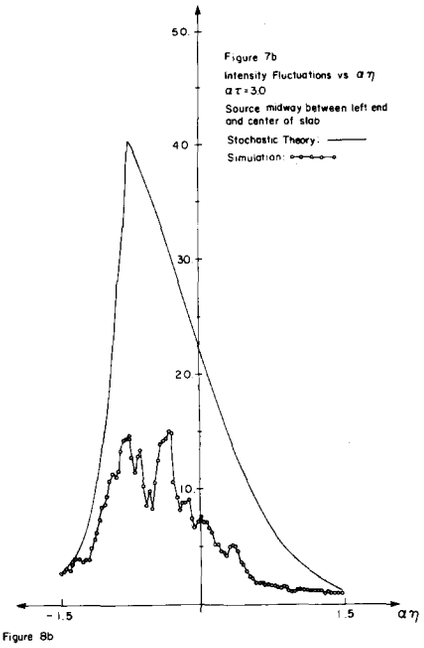

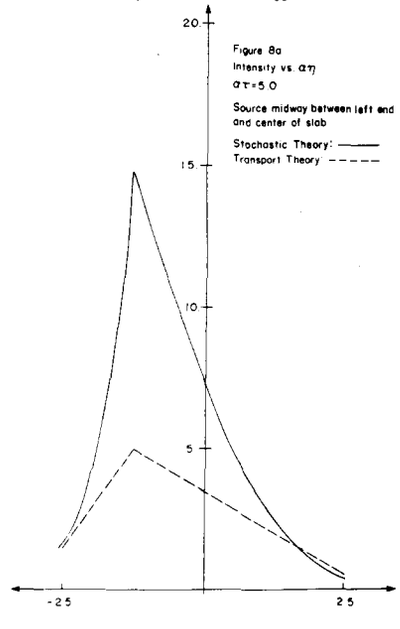

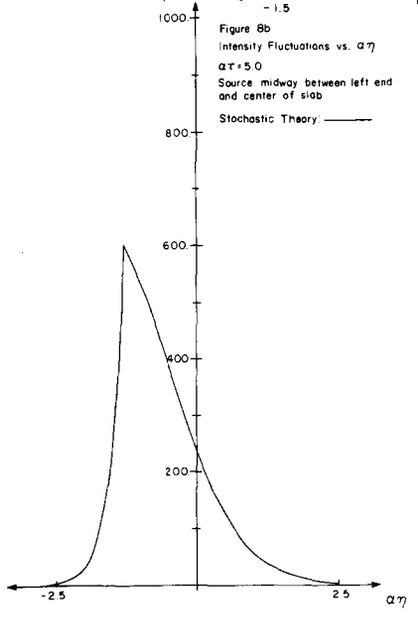

FIGS. 5—8.

(2.21); the transport theoretic transmission coefficient can be obtained by setting $\xi = -\tau/2$ in (3.5). We have

$$MJ_s(\tau, \tau/2, \tau/2) = 1/(1+\alpha\tau). \tag{3.11}$$

The stochastic transmission coefficient decreases exponentially while the transport theoretic transmission coefficient decreases algebraically. The fluctuations also decrease with increasing $\alpha\tau$. As $\alpha\tau$ increases, therefore, the transmission coefficient approaches zero in probability. This behavior has also been established by Sulem and Frisch[20] when the index of refraction is a random telegraph process and, in fact, convergence is with probability one. For values of $\alpha\tau$ greater than 8, the fluctuations are less than the corresponding spread between stochastic and transport theory intensity predictions. In the light of these observations, one would expect reasonably good agreement between stochastic theory predictions and numerical simulation at the right end of the slab. Moreover, the simulated results should discriminate between the two theories. Simulation results of this sort have been reported by Morrison.[21] The simulations plotted in Figures 1—4 and 13 also behave in this anticipated manner.

In performing the numerical simulations, the expected values were approximated by computing an average over 100 realizations. Each of these realizations in turn was a slab consisting of 2000 sections (i.e., of unscaled length 2000). Within each realization, the index of refraction was assumed to be a two-state random process, with states $\sqrt{1\pm\epsilon}$. The initial state (i.e., the value of the process at the left end of the slab) was chosen randomly; subsequent switching of states occured randomly at intervals which were (approximately) exponentially distributed. In the computations, the average number of sections between changes of the index of refraction was varied from 2.5 to 10, while a wavenumber of 0.5 was used throughout. The parameter ϵ, therefore, was not specified directly but rather was determined by the other variables. Typically, ϵ fell within the range $0.1 \leq \epsilon \leq 0.3$.

The simulations were beset by two difficulties, the strongly fluctuating nature of the process being simulated and the inherent limitations of the discrete approximating model. Note, in particular, the failure of the simulation model to generate the fluctuations predicted in Figs. 7b and 11b. In general, however, the agreement between the simulated results and stochastic theory is good, and we feel that these simulations amply demonstrate the applicability of the stochastic theory.

Throughout this discussion, we have assumed that frequency (or wavenumber k) is fixed while the spatial variables change. Note, however, from (2.21)—(2.24), (3.4) and the graphs, that MJ, FJ, and MJ_s are functions of $\alpha\tau$, $\alpha\xi$, and $\alpha\eta$, where α is defined by (2.18). Consequently, we could equally well adopt the point of view that the spatial variables are fixed and wavenumber is variable. For fixed τ, ξ, η and a particular correlation function, we could use our graphical data to determine the variation of MJ, FJ, and MJ_s as functions of wavenumber through $\alpha(k)$; observe from (2.1), however, that we would have to account for the fact that our source strength is frequency-dependent.

4. DERIVATION OF THE RESULTS

The derivation that we shall present will rely on Secs. 3—6 of I. In addition to the theory of Ref. 3 (Theorem 3 of Ref. 3) which we used in I, we shall now also apply an improved version of that theory.[4] For the problem being considered, we need the improved theory to conclude that the limit theorem for the propagator matrices (Sec. 4 of I) holds for certain unbounded functions of these matrices. In fact, in I the condition of Theorem 3 (Ref. 3) that $f(g)$ be bounded was violated. With the improved theory, however, such conditions are no longer needed. Hence, the results of I, up to Sec. 9, are rigorously correct. The pulse propagation results of Sec. 9, though, still require additional theoretical considerations because of complications that were overlooked; we shall not pursue this matter here. In the analysis that follows we shall point out where the improved theory is needed.

Let $m(x)$ denote the 2×2 matrix-valued stochastic process:

$$m(x) = \frac{ik\mu(x)}{2}\begin{pmatrix} 1 & \exp(-i2kx) \\ -\exp(i2kx) & -1 \end{pmatrix}. \tag{4.1}$$

Let η_1, η_2, η_3 be defined as the following 2×2 matrices:

$$\eta_1 = \tfrac{1}{2}\begin{pmatrix} i & 0 \\ 0 & -i \end{pmatrix}, \quad \eta_2 = \tfrac{1}{2}\begin{pmatrix} 0 & 1 \\ 1 & 0 \end{pmatrix}, \quad \eta_3 = \tfrac{1}{2}\begin{pmatrix} 0 & i \\ -i & 0 \end{pmatrix}. \tag{4.2}$$

We can express $m(x)$ in terms of η_1, η_2, η_3 as follows:

$$m(x) = k\mu(x)\eta_1 + (k\mu(x)\sin 2kx)\eta_2 + (k\mu(x)\cos 2kx)\eta_3. \tag{4.3}$$

Note that η_1, η_2, and η_3 constitute a representation of the Lie algebra $su(1,1)$ with commutation relations

$$\eta_1\eta_2 - \eta_2\eta_1 = [\eta_1, \eta_2] = \eta_3, \quad [\eta_1, \eta_3] = -\eta_2,$$
$$[\eta_2, \eta_3] = -\eta_1. \tag{4.4}$$

Thus, $m(x)$ is a stochastic process with values in $su(1,1)$.

Let $Y(x,y)$ denote the 2×2 matrix solution of the initial value problem:

$$\frac{dY}{dx}(x,y) = \epsilon m(x) Y(x,y),$$
$$Y(y,y) = I \text{ (}2\times 2\text{ identity matrix)}, \quad x \geq y. \tag{4.5}$$

In view of (4.3), $Y(x,y)$ is a stochastic process with values in $SU(1,1)$, the group of 2×2 matrices of the form

$$Y = \begin{pmatrix} a & b \\ \bar{b} & \bar{a} \end{pmatrix}, \quad |a|^2 - |b|^2 = 1. \tag{4.6}$$

We decompose $Y(l,0)$ into the product

$$Y(l,0) = Y_3(l,y)Y_2(y,x)Y_1(x,0), \quad 0 \leq x \leq y \leq l,$$
$$Y(l,0) = Y_3(l,x)Y_2(x,y)Y_1(y,0), \quad 0 \leq y \leq x \leq l. \tag{4.7}$$

The matrices Y_1, Y_2, and Y_3, when viewed as functions of their first argument, are solutions of (4.5) which equal the identity matrix when their two arguments coincide. Equation (4.7) is simply an expression of the propagator property (cf. I, Sec. 3). To simplify the notation, we omit the arguments and write

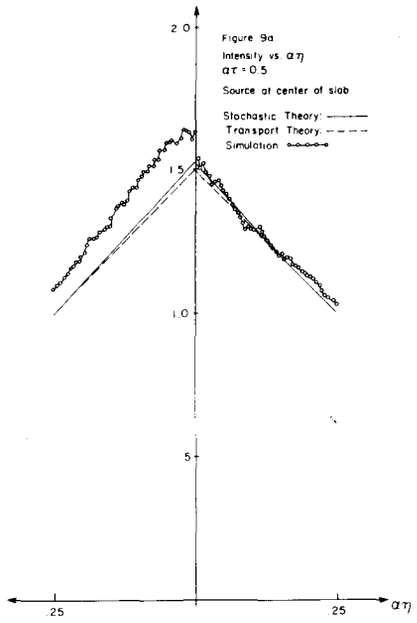

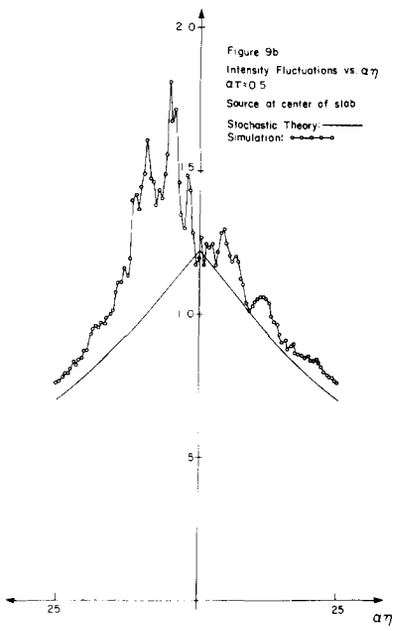

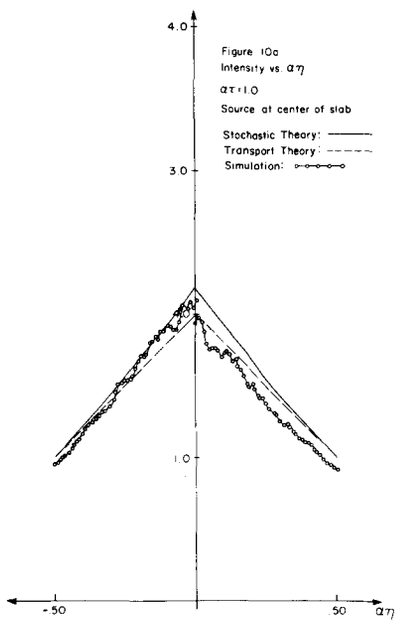

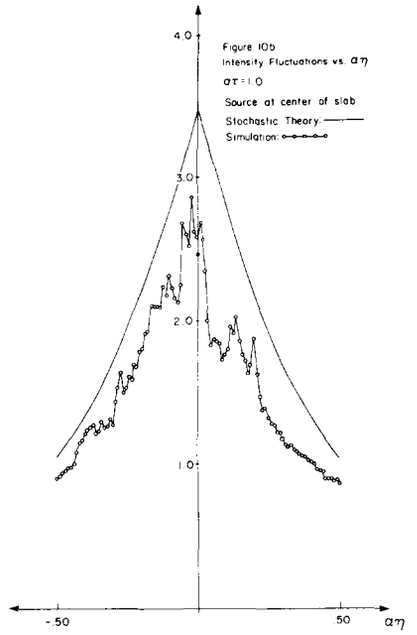

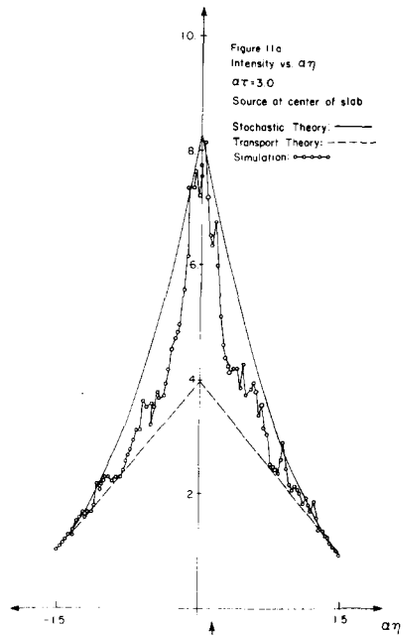

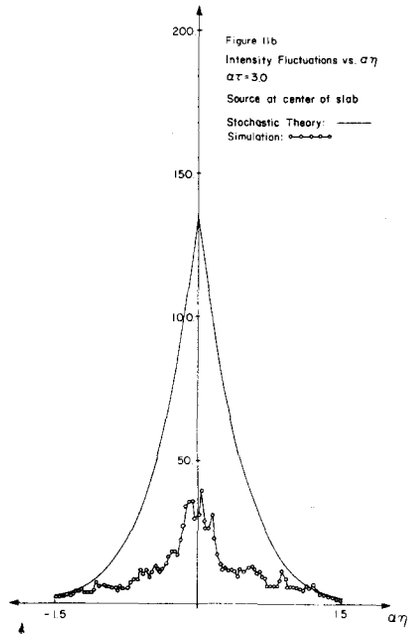

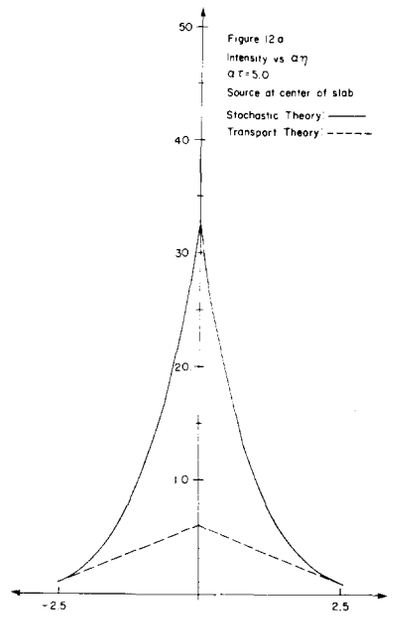

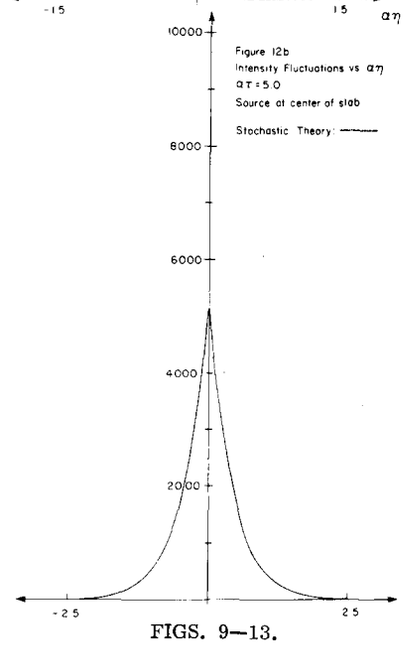

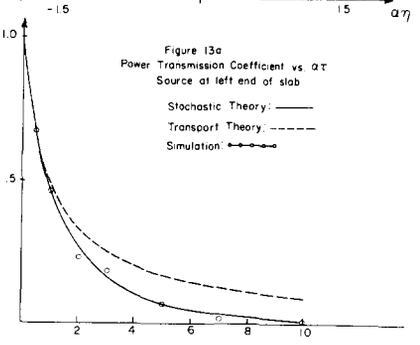

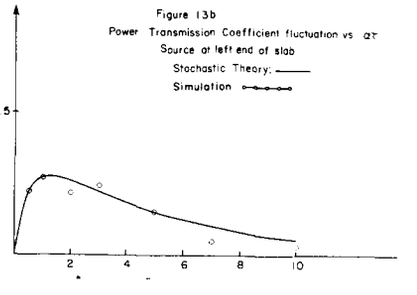

FIGS. 9—13.

$$Y_j=\begin{pmatrix} a_j & b_j \\ \bar{b}_j & \bar{a}_j \end{pmatrix}, \quad |a_j|^2-|b_j|^2=1, \quad j=1,2,3. \tag{4.8}$$

The solution of boundary value problem (2.7)—(2.9) can be expressed in terms of Y_1, Y_2, and Y_3 as follows:

$$\left.\begin{aligned} A&=\frac{b_1[\bar{a}_3\exp(iky)-\bar{b}_3\exp(-iky)]}{\bar{b}_3(a_2b_1+b_2\bar{a}_1)+\bar{a}_3(\bar{b}_2b_1+\bar{a}_2\bar{a}_1)} \\ B&=\frac{-\bar{a}_1[\bar{a}_3\exp(iky)-\bar{b}_3\exp(-iky)]}{\bar{b}_3(a_2b_1+b_2\bar{a}_1)+\bar{a}_3(\bar{b}_2b_1+\bar{a}_2\bar{a}_1)} \end{aligned}\right\}, \quad 0\le x\le y\le l, \tag{4.9}$$

$$\left.\begin{aligned} A&=\frac{\bar{a}_3[\bar{a}_1\exp(-iky)+b_1\exp(iky)]}{b_1(\bar{b}_2\bar{a}_3+a_2\bar{b}_3)+\bar{a}_1(b_2\bar{b}_3+\bar{a}_2\bar{a}_3)} \\ B&=\frac{-b_3[\bar{a}_1\exp(-iky)+b_1\exp(iky)]}{b_1(\bar{b}_2\bar{a}_3+a_2\bar{b}_3)+\bar{a}_1(b_2\bar{b}_3+\bar{a}_2\bar{a}_3)} \end{aligned}\right\}, \quad 0\le y\le x\le l. \tag{4.10}$$

These formulas generalize (I. 3.9) and (I. 3.10) for the matched case.

We shall now introduce the notation:

$$\begin{pmatrix} a_{21} & b_{21} \\ \bar{b}_{21} & \bar{a}_{21} \end{pmatrix}=\begin{pmatrix} a_2 & b_2 \\ \bar{b}_2 & \bar{a}_2 \end{pmatrix}\begin{pmatrix} a_1 & b_1 \\ \bar{b}_1 & \bar{a}_1 \end{pmatrix}=\begin{pmatrix} a_2a_1+b_2b_1 & a_2\bar{b}_1+b_2\bar{a}_1 \\ \bar{b}_2a_1+\bar{a}_2\bar{b}_1 & \bar{b}_2b_1+\bar{a}_2\bar{a}_1 \end{pmatrix}, \tag{4.11}$$

$$\begin{pmatrix} a_{32} & b_{32} \\ \bar{b}_{32} & \bar{a}_{32} \end{pmatrix}=\begin{pmatrix} a_3 & b_3 \\ \bar{b}_3 & \bar{a}_3 \end{pmatrix}\begin{pmatrix} a_2 & b_2 \\ \bar{b}_2 & \bar{a}_2 \end{pmatrix}=\begin{pmatrix} a_3a_2+b_3\bar{b}_2 & a_3b_2+b_3\bar{a}_2 \\ \bar{b}_3a_2+\bar{a}_3\bar{b}_2 & \bar{b}_3b_2+\bar{a}_3\bar{a}_2 \end{pmatrix}. \tag{4.12}$$

Observe that the denominator of (4.9) is $\bar{b}_3b_{21}+\bar{a}_3\bar{a}_{21}$ and the denominator of (4.10) is $b_1\bar{b}_{32}+\bar{a}_1\bar{a}_{32}$. We shall also introduce polar coordinates, as in Sec. 5 of I, by defining

$$\begin{aligned} a_j&=\exp[i(\phi_j+\psi_j)/2]\cosh(\theta_j/2), \\ b_j&=\exp[i(\phi_j-\psi_j)/2]\sinh(\theta_j/2), \\ j&=1,2,3. \end{aligned} \tag{4.13}$$

Similarly, let

$$\begin{aligned} a_{21}&=\exp[i(\phi_{21}+\psi_{21})/2]\cosh(\theta_{21}/2), \\ b_{21}&=\exp[i(\phi_{21}-\psi_{21})/2]\sinh(\theta_{21}/2), \\ a_{32}&=\exp[i(\phi_{32}+\psi_{32})/2]\cosh(\theta_{32}/2), \\ b_{32}&=\exp[i(\phi_{32}-\psi_{32})/2]\sinh(\theta_{32}/2). \end{aligned} \tag{4.14}$$

The following useful relations, which constitute the law of cosines in the hyperbolic disc, are a consequence of (4.11) and (4.12):

$$\begin{aligned} \cosh\theta_{21}&=\cosh\theta_1\cosh\theta_2+\cos(\phi_1+\psi_2)\sinh\theta_1\sinh\theta_2, \\ \cosh\theta_{32}&=\cosh\theta_2\cosh\theta_3+\cos(\phi_2+\psi_3)\sinh\theta_2\sinh\theta_3. \end{aligned} \tag{4.15}$$

We are primarily interested in $J^{(\epsilon)}(x,y,l)$, which is defined by (2.12). Using (4.9)—(4.16), we express it as the following function of the polar coordinates:

$$J^{(\epsilon)}(x,y,l)$$

$$=\frac{2\cosh\theta_1[\cosh\theta_3-\cos(2ky-\psi_3)\sinh\theta_3]}{1+\cosh\theta_3\cosh\theta_{21}+\cos(\psi_3+\phi_{21})\sinh\theta_3\sinh\theta_{21}}, \quad 0\le x\le y\le l, \tag{4.16}$$

$$J^{(\epsilon)}(x,y,l)$$

$$=\frac{2\cosh\theta_3[\cosh\theta_1+\cos(2ky+\phi_1)\sinh\theta_1]}{1+\cosh\theta_1\cosh\theta_{32}+\cos(\phi_1+\psi_{32})\sinh\theta_1\sinh\theta_{32}}, \quad 0\le y\le x\le l. \tag{4.17}$$

These formulas generalize (I. 5.12) and (I. 5.13) for the matched case.

Note that

$$|J^{(\epsilon)}(x,y,l)|\le\cosh\theta_1(\cosh\theta_3+|\sinh\theta_3|), \quad 0\le x\le y\le l, \tag{4.18}$$

or

$$|J^{(\epsilon)}(x,y,l)|\le\cosh\theta_3(\cosh\theta_1+|\sinh\theta_1|), \quad 0\le y\le x\le l. \tag{4.19}$$

From (4.13) it follows that:

$$|J^{(\epsilon)}(x,y,l)|\le(|a_1|^2+|b_1|^2)(|a_3|+|b_3|)^2, \quad 0\le x\le y\le l, \tag{4.20}$$

$$|J^{(\epsilon)}(x,y,l)|\le(|a_3|^2+|b_3|^2)(|a_1|+|b_1|)^2 \quad 0\le y\le x\le l. \tag{4.21}$$

$J^{(\epsilon)}$ can therefore be bounded by absolute moments of the elements of the propagator matrices. These are precisely the kind of estimates required in the improved theory of Ref. 4. Theorem 3 of Ref. 3, on the other hand required uniform boundedness. We can thus proceed now as in Secs. 4 and 5 of I without difficulty.

To facilitate application of the limit theorem, expressions (4.18) and (4.19) for $J^{(\epsilon)}$ will be further transformed. We record the following facts about the Legendre functions $P_\nu^m(u)$ that are needed[22]:

$$\frac{d}{du}\left((u^2-1)\frac{d}{du}P_\nu^m(u)\right)-\frac{m^2}{u^2-1}P_\nu^m(u) =\nu(\nu+1)P_\nu^m(u), \quad u>1, \tag{4.22}$$

$$\frac{2}{u+1}=\int_{-\infty}^{\infty}\frac{\pi t\sinh\pi t}{\cosh^2\pi t}P_{-1/2+it}(u)\,dt, \tag{4.23}$$

$$P_\nu(\cosh\xi)=\sum_{m=-\infty}^{\infty}\frac{\Gamma(\nu-|m|+1)}{\Gamma(\nu+|m|+1)}P_\nu^{|m|}(\cosh\theta) \times P_\nu^{|m|}(\cosh\tilde{\theta})\exp[im(\phi+\psi)], \tag{4.24}$$

$$\cosh\xi=\cosh\theta\cosh\tilde{\theta}+\cos(\phi+\psi)\sinh\theta\sinh\tilde{\theta}, \tag{4.25}$$

$$P_\nu^m(u)=P_{-\nu-1}^m(u), \tag{4.26}$$

$$uP_\nu^{|m|}(u)=\frac{1}{2\nu+1}[(\nu-|m|+1)P_{\nu+1}^{|m|}(u) +(\nu+|m|)P_{\nu-1}^{|m|}(u)], \tag{4.27}$$

$$\frac{4}{(u+1)^2}=\int_{-\infty}^{\infty}(t^2+\tfrac{1}{4})\frac{\pi t\sinh\pi t}{\cosh^2\pi t}P_{-1/2+it}(u)\,dt, \quad u\ge1. \tag{4.28}$$

Only (4.23) and (4.28) require a brief comment. Note that if we set $u=1$ and use the fact that $P_\nu(1)=1$, we obtain the relations $\beta_0=1$ and $\beta_1+\frac{1}{4}\beta_0=1$, respectively [cf. (3.7)]. It is well known that (4.23) follows from the Mehler transform.[22] We can derive (4.28) from (4.23) by observing that the solution $g(\tau,u)$ of the equation

$$\frac{\partial}{\partial\tau}g=\frac{\partial}{\partial u}\left((u^2-1)\frac{\partial}{\partial u}g\right), \quad u>1, \quad g(0,u)=\frac{1}{1+u} \tag{4.29}$$

has the integral representation

$$g(\tau,u)=\int_0^\infty \exp[-(t^2+\tfrac{1}{4})\tau]P_{-1/2+it}(u)\frac{\pi t\sinh\pi t}{\cosh^2\pi t}\,dt. \quad (4.30)$$

Therefore, we have

$$g_\tau(0,u)=\left[(u^2-1)\left(\frac{1}{1+u}\right)'\right]'=\frac{-2}{(1+u)^2}. \quad (4.31)$$

By combining (4.31) and (4.30), we obtain (4.28).

We shall analyze (4.16) in detail; the analysis of (4.17) follows in the same way. Observe that we can write

$$\cosh\theta_{321}=\cosh\theta_3\cosh\theta_{21}+\cos(\psi_3+\phi_{21})\sinh\theta_3\sinh\theta_{21}, \quad (4.32)$$

where the triple subscript is an obvious extension of the notation introduced in (4.14) and (4.15). By using (4.23), Eq. (4.16) can be rewritten as follows:

$$J^{(\epsilon)}=\cosh\theta_1[\cosh\theta_3-\cos(2ky-\psi_3)\sinh\theta_3]\int_{-\infty}^{\infty}\frac{\pi t\sinh\pi t}{\cosh^2\pi t}\times P_{-1/2+it}(\cosh\theta_{321})\,dt,\quad 0\le x\le y\le l. \quad (4.33)$$

Addition theorem (4.24) when applied to (4 yields

$$J^{(\epsilon)}=\cosh\theta_1[\cosh\theta_3-\cos(2ky-\psi_3)\sinh\theta_3]\int_{-\infty}^{\infty}\frac{\pi t\sinh\pi t}{\cosh^2\pi t}\times\left(\sum_{m=-\infty}^{\infty}\frac{\Gamma(\nu-|m|+1)}{\Gamma(\nu+|m|+1)}P_\nu^{|m|}(\cosh\theta_3)P_\nu^{|m|}(\cosh\theta_{21})\times\exp(im(\phi_{21}+\psi_3))\right)dt,\quad \nu=-\tfrac{1}{2}+it \quad (4.34)$$

To decompose $P_\nu^{|m|}(\cosh\theta_{21})$, we require a generalization of addition theorem (4.24). This, in turn, necessitates the introduction of generalized Legendre functions. All necessary information about such functions, including addition theorems and recurrence relations, is given by Vilenkin[23] (in Chap. VI). We record here the required addition theorem:

$$\exp(im\phi_{21})\,P_\nu^{|m|}(\cosh\theta_{21})=\sum_{n=-\infty}^{\infty}\frac{\Gamma(\nu+|m|+1)}{\Gamma(\nu+n+1)}\exp(-in(\phi_1+\psi_2)+im\phi_2)\times P^\nu_{|m|,n}(\cosh\theta_2)\,P_\nu^n(\cosh\theta_1). \quad (4.35)$$

The generalized Legendre function P^ν_{mn} satisfies the differential equation:

$$\frac{d}{du}\left((u^2-1)\frac{d}{du}P^\nu_{mn}(u)\right)-\left(\frac{m^2+n^2-2mnu}{u^2-1}\right)P^\nu_{mn}(u)=\nu(\nu+1)\,P^\nu_{mn}(u),\quad u>1, \quad (4.36)$$

and also the relation

$$P^\nu_{0n}(\cosh\theta)=\frac{\Gamma(\nu-n+1)}{\Gamma(\nu+1)}P_\nu^m(\cosh\theta). \quad (4.37)$$

Therefore, when $m=0$, addition theorem (4.35) reduces to (4.24).

We now use (4.35) in (4.34) to obtain the desired representation for $J^{(\epsilon)}$ (when $0\le x\le y\le l$):

$$J^{(\epsilon)}=\cosh\theta_1[\cosh\theta_3-\cos(2ky-\psi_3)\sinh\theta_3]\int_{-\infty}^{\infty}\frac{\pi t\sinh\pi t}{\cosh^2\pi t}\times\left(\sum_{m=-\infty}^{\infty}\sum_{n=-\infty}^{\infty}\frac{\Gamma(\nu-|m|+1)}{\Gamma(\nu+n+1)}\exp(im(\phi_2+\psi_3))\exp(-in(\phi_1+\psi_2))\times P_\nu^n(\cosh\theta_1)\,P^\nu_{|m|,n}(\cosh\theta_2)\,P_\nu^{|m|}(\cosh\theta_3)\right)dt,\quad \nu=-\tfrac{1}{2}+it. \quad (4.38)$$

A similar analysis, utilizing (4.28), can be performed to obtain the following representation for $(J^{(\epsilon)})^2$ (when $0\le x\le y\le l$)

$$(J^{(\epsilon)})^2=\cosh^2\theta_1[\cosh\theta_3-\cos(2ky-\psi_3)\sinh\theta_3]^2\int_{-\infty}^{\infty}(t^2+\tfrac{1}{4})\times\frac{\pi t\sinh\pi t}{\cosh^2\pi t}\left(\sum_{m=-\infty}^{\infty}\sum_{n=-\infty}^{\infty}\frac{\Gamma(\nu-|m|+1)}{\Gamma(\nu+n+1)}\exp(im(\phi_2+\psi_3))\times\exp(-in(\phi_1+\psi_2))\,P_\nu^n(\cosh\theta_1)\,P^\nu_{|m|,n}(\cosh\theta_2)\times P_\nu^{|m|}(\cosh\theta_3)\right)dt,\quad \nu=-\tfrac{1}{2}+it. \quad (4.39)$$

We now apply the diffusion limit, i.e., (2.16) and (2.22), to (4.38) and (4.39) to obtain MJ and KJ, respectively. Thus, we take expectation or statistical average of $J^{(\epsilon)}$ and $(J^{(\epsilon)})^2$ with respect to the limiting probability distribution of the propagators. As explained in Sec. 4 of I, the propagator matrices corresponding to nonoverlapping intervals become statistically independent in the diffusion limit. Up to this point, our analysis could be applied to the mismatched problem by adjusting the initial value of Y_1 and the final value of Y_3 (cf. Sec. 3 of I). In the sequel, we shall consider only the matched case; the formulas for the more general mismatched case are unwieldy but not particularly difficult to obtain.

Observe that the angle ψ_1 is absent in both (4.38) and (4.39). As explained in Sec. 5 of I, the limiting transition density for ϕ is uniformly distributed over $[0,2\pi]$ and is independent of θ_1. (Recall that we are dealing with the matched case.) Therefore, when we average (4.38) and (4.39) with respect to ϕ_1, only the $n=0$ term survives. Moreover, since ψ_2 appears only in the combination $(\phi_1+\psi_2)$, this average with respect to ϕ_1 also eliminates functional dependence upon ψ_2. We next average with respect to ϕ_2. The same argument applies to this case also; the transition density for ϕ_2 is uniformly distributed over $[0,2\pi]$ and independent of θ_2. When this average is performed, only the $m=0$ term survives. We next average with respect to the uniformly distributed angle ψ_3. If we use angular brackets $\langle\cdot\rangle$ to denote averaging with respect to the angles ϕ_1, ϕ_2, and ψ_3, then (4.38) and (4.39) yield

$$\langle J\rangle=\cosh\theta_1\cosh\theta_3\int_{-\infty}^{\infty}\frac{\pi t\sinh\pi t}{\cosh^2\pi t}P_\nu(\cosh\theta_1)\times P_\nu(\cosh\theta_2)\,P_\nu(\cosh\theta_3)\,dt, \quad (4.40)$$

$$\langle J^2\rangle=\cosh^2\theta_1\left(\frac{3\cosh^2\theta_3-1}{2}\right)\int_{-\infty}^{\infty}(t^2+\tfrac{1}{4})\frac{\pi t\sinh\pi t}{\cosh^2\pi t}P_\nu(\cosh\theta_1)\times P_\nu(\cosh\theta_2)P_\nu(\cosh\theta_3)\,dt,\quad \nu=-\tfrac{1}{2}+it. \quad (4.41)$$

To obtain MJ and KJ, we must average (4.40) and (4.41) with respect to the limiting distributions of θ_1, θ_2, and θ_3. Since we are in the matched case, it follows from (I. 5.21) [or directly from (I. 5.16)] that in the diffusion limit

$$E\{P_\nu(\cosh\theta(\tau))\} = \exp(\nu(\nu+1)\alpha\tau). \tag{4.42}$$

In (4.40) and (4.41) we must take the expected value of functions of the form $u^j P_\nu(u)$, $j=0,1,2$, where $u=\cosh\theta$. Notice, however, that by using (4.26) and (4.27) we can rewrite $uP_\nu(u)$ and $u^2P_\nu(u)$ as linear combination of Legendre functions with different degrees. We use the scaled variables defined by (2.15) in specifying the arguments of the random functions θ_1, θ_2, and θ_3. For the case being considered, i.e., $0 \leq x \leq y \leq l$, these arguments are $\tau/2+\eta$, $\xi-\eta$ and $\tau/2-\xi$, respectively. Equation (4.42) is used repeatedly and after some straightforward but lengthy computations, (2.17) is obtained from (4.40) and (2.24) from (4.41). By starting with (4.17), the analysis for the other case, i.e., $0 \leq y \leq x \leq l$, follows in basically the same way as the case we have discussed.

Gazaryan[7] studied the configuration corresponding to the matched case with a source location at the left end of the slab ($\xi=-\tau/2$). He observed that the total intensity in the interior, i.e., $MJ(\tau,-\tau/2,\eta)$, satisfies the heat equation in the variables τ and η. Moreover, Eq. (2.19) with $\tau=0$, can be recast into the following very simple initial condition:

$$MJ(0,0,\eta) = 1-\tanh\alpha\eta-\alpha\eta\,\mathrm{sech}^2\alpha\eta. \tag{4.43}$$

Using the fundamental solution to the heat equation, Gazaryan obtained an alternate representation for $MJ(\tau,-\tau/2,\eta)$. His observation was generalized and used extensively in Sec. 6 of I.

For the general configuration, where the source location is permitted to vary, one can show that $MJ(\tau,\xi,\eta)$ satisfies the following partial differential equation:

$$\partial_{\alpha\tau}MJ = \tfrac{1}{4}[\tfrac{1}{2}(\partial^2_{\alpha\eta,\alpha\eta}+\partial^2_{\alpha\xi,\alpha\xi})-\sigma(\partial_{\alpha\eta}-\partial_{\alpha\xi})]MJ,$$
$$\sigma=\mathrm{sgn}(\eta-\xi). \tag{4.44}$$

However, KJ does not satisfy such a simple partial differential equation. Moreover, the simplicity of the approach as a whole is apparently lost in this more general problem. Consequently, the approach was not pursued.

ACKNOWLEDGMENT

We wish to thank Uriel Frisch for bringing the interior source problem to our attention and J.B. Keller for useful comments and suggestions.

*Research supported by the Air Force Office of Scientific Research under Grant No. AFOSR-71-2013.

[1]W. Kohler and G.C. Papanicolaou, J. Math. Phys. **14**, 1733 (1973).
[2]G.C. Papanicolaou and J.B. Keller, SIAM J. Appl. Math. (Soc. Ind. Appl. Math.) **21**, 287 (1971).
[3]G.C. Papanicolaou and S.R.S. Varadhan, Comm. Pure Appl. Math. **26**, 497 (1973).
[4]G.C. Papanicolaou and W. Kohler, Comm. Pure Appl. Math. **27**, (1974) (to be published).
[5]J.A. Morrison and J. McKenna, SIAM—AMS Proc. 6, 97 (1973).
[6]A. Brissaud and U. Frisch, J. Math. Phys. **15**, 524 (1974).
[7]Yu.L. Gazaryan, Zh. Eksp. Teor. Fiz. **56**, 1856 (1969) [Sov. Phys. JETP **29**, 996 (1969)].
[8]R.H. Lang, J. Math. Phys. **14**, 1921 (1973).
[9]R.J. Rubin, J. Math. Phys. **9**, 2252 (1968).
[10]R.J. Rubin, J. Math. Phys. **11**, 1857 (1970).
[11]B.I. Halperin, Phys. Rev. **139**, A104 (1965).
[12]D. Marcuse, Bell Sys. Tech. J. **51**, 1793 (1972).
[13]A. Schuster, Astrophys. J. **21**, 1 (1905).
[14]I.M. Besieris and F.D. Tappert, J. Appl. Phys. **44**, 2119 (1973).
[15]For the validity of the diffusion limit it is required that $\mu(x)$ be almost surely bounded and mixing in a sufficiently strong sense (cf. Refs. 1, 3, and 4). Model media with $\mu(x)$ a finite state ergodic Markov chain are included in our formulation.
[16]This denotes Eq. (2.15) in I.
[17]The leading minus sign on the third line of (I.6.32) should be a plus sign.
[18]D. Marcuse, IEEE Trans. MTT **20**, 541 (1972).
[19]U. Frisch, C. Froeschle, J.-P. Scheidecker, and P.L. Sulem, Phys. Rev. A **8**, 1416 (1973).
[20]P.L. Sulem and U. Frisch, J. Plasma Phys. **8**, 217 (1972).
[21]J.A. Morrison, IEEE Trans. MTT **22**, 126 (1974).
[22]W. Magnus, F. Oberhettinger and R.P. Soni, *Formulas and Theorems for the Special Functions of Mathematical Physics* (Springer, New York, 1966).
[23]N.J. Vilenkin, *Special Functions and the Theory of Group Representations*, 22, Transl. of Math. Monographs (AMS, Providence, R.I., 1968).